THE JOURNAL OF BIOLOGICAL CHEMISTRY VOL. 281, NO. 14, pp. 9471–9481, April 7, 2006

Asparagine 706 and Glutamate 183 at the Catalytic Site of Sarcoplasmic Reticulum Ca^{2+}-ATPase Play Critical but Distinct Roles in *E*2 States*[S]

Received for publication, November 17, 2005, and in revised form, January 24, 2006 Published, JBC Papers in Press, January 30, 2006, DOI 10.1074/jbc.M512371200

Johannes D. Clausen[‡], David B. McIntosh[§], David G. Woolley[§], Anne Nyholm Anthonisen[‡], Bente Vilsen[‡], and Jens Peter Andersen[‡1]

From the [‡]Department of Physiology, Institute of Physiology and Biophysics, University of Aarhus, DK-8000 Aarhus C, Denmark and the [§]Institute of Infectious Disease and Molecular Medicine, Faculty of Health Sciences, University of Cape Town, Observatory, Cape Town 7925, South Africa

Mutants with alteration to Asn^{706} of the highly conserved ^{701}TGDGVND^{707} motif in domain P of sarcoplasmic reticulum Ca^{2+}-ATPase were analyzed for changes in transport cycle kinetics and binding of the inhibitors vanadate, BeF, AlF, and MgF. The fluorides likely mimic the phosphoryl group/P_i in the respective ground, transition, and product states of phosphoenzyme hydrolysis (Danko, S., Yamasaki, K., Daiho, T., and Suzuki, H. (2004) *J. Biol. Chem.* 279, 14991–14998). Binding of BeF, AlF, and MgF was also studied for mutant $Glu^{183} \rightarrow$ Ala, where the glutamate of the ^{181}TGES^{184} motif in domain A is replaced. Mutations of Asn^{706} and Glu^{183} have in common that they dramatically impede the function of the enzyme in *E*2 states, but have little effect in *E*1. Contrary to the Glu^{183} mutant, in which *E*2P slowly accumulates (Clausen, J. D., Vilsen, B., McIntosh, D. B., Einholm, A. P., and Andersen, J. P. (2004) *Proc. Natl. Acad. Sci. U. S. A.* 101, 2776–2781), *E*2P formation was not detectable with the Asn^{706} mutants. Differential sensitivities of the mutants to inhibition by AlF, MgF, and BeF made it possible to distinguish different roles of Asn^{706} and Glu^{183}. Hence, Asn^{706} is less important than Glu^{183} for gaining the transition state during *E*2P hydrolysis but plays critical roles in stabilization of *E*2P ground and *E*2·P_i product states and in the major conformational changes associated with the Ca_2*E*1P → *E*2P and *E*2 → Ca_2*E*1 transitions, which seem to be facilitated by interaction of Asn^{706} with domain A.

The sarco(endo)plasmic reticulum Ca^{2+}-ATPase (1) is an energy-transducing enzyme of the P-type that couples hydrolysis of ATP to translocation of Ca^{2+} from the cytosol to the endoplasmic reticulum. In this control of cytosolic Ca^{2+} concentration, the Ca^{2+}-ATPase plays a vital role in cellular activation events, such as muscle contraction, hormone secretion, immune responses, cell migration, and protein synthesis. Ca^{2+} transport is coupled to ATP hydrolysis by a reaction cycle (Scheme 1), in which the enzyme is transiently phosphorylated at a conserved aspartic acid residue and undergoes major conformational changes (2, 3).

In recent years, several high resolution crystal structures of the Ca^{2+}-ATPase, each thought to represent a particular intermediate state in the pump cycle, have been solved (4–9). The Ca^{2+}-ATPase consists of a membrane-spanning domain of ten helical segments and a large cytoplasmic head piece, comprising three distinct domains, named "N" (nucleotide binding), "P" (phosphorylation), and "A" (actuator). By combining crystallographic data with functional changes in site-specific mutants, an increasingly detailed picture of the mechanisms of energy interconversion and ion translocation in the Ca^{2+}-ATPase is emerging. Thus, the catalytic function in *E*1 (autokinase activity) and *E*2 forms (autophosphatase activity), the movement of Ca^{2+} ions across the membrane, as well as the major rate-limiting conformational changes of the cycle, *i.e.* *E*2 → *E*1 and *E*1P → *E*2P, can all be understood on the basis of the sequential gathering and displacement of certain conserved amino acid motifs in domains N and A relative to the catalytic site in domain P and the coupling of these events to rearrangements of the transmembrane helices containing the high affinity Ca^{2+} sites.

In the present study, we address the role of Asn^{706} at the catalytic site of Ca^{2+}-ATPase and revisit a previously examined mutant, E183A (10). Asn^{706} and Glu^{183} reside in the conserved ^{701}TGDGVND^{707} (domain P) and ^{181}TGES^{184} (domain A) motifs, respectively, and both residues are found in all known P-type ATPases (11). In fact, Asn^{706} is highly conserved even in the superfamily of phosphohydrolases and phosphotransferases (the HAD superfamily), which, given the similarities in reaction mechanism, protein sequence, and structural architecture of the catalytic site, are believed to share a common evolutionary ancestor with the phosphorylation domain of the P-type ATPases (12–14). The side chains of Asn^{706} and Glu^{183} are both centrally located at the catalytic site in the *E*2 forms of Ca^{2+}-ATPase, close to the phosphorylated aspartate, Asp^{351} (6, 7, 9). In *E*1 conformations, Glu^{183} has departed the phosphorylation site, whereas Asn^{706} retains its close proximity to Asp^{351} (4, 5, 7, 8). In our previous study of Glu^{183} (10), we demonstrated that substitution of the glutamate with alanine leads to a much reduced rate of both *E*2P hydrolysis and of the reverse phosphorylation of *E*2 with P_i, suggesting that Glu^{183} is critical for *E*2P transition state stabilization and catalysis. This proved to correlate well with the subsequently published *E*2·AlF[2] crystal structure, in which Glu^{183} seems to coordinate and likely activates the attacking water molecule in the transition

* This work was funded in part by grants from the Danish Medical Research Council, the Novo Nordisk Foundation, Denmark, the Lundbeck Foundation, Denmark, the Research Foundation of Aarhus University (to J. P. A.), the Carlsberg Foundation, Denmark (to J. D. C.), and the National Research Foundation of South Africa (to D. B. M.). The costs of publication of this article were defrayed in part by the payment of page charges. This article must therefore be hereby marked "*advertisement*" in accordance with 18 U.S.C. Section 1734 solely to indicate this fact.

[S] The on-line version of this article (available at http://www.jbc.org) contains supplemental Figs. S1 and S11.

[1] To whom correspondence should be addressed. Tel.: 45-89-42-28-14; Fax: 45-86-12-90-65; E-mail: jpa@fi.au.dk.

[2] The abbreviations used are: AlF, complex of Al^{3+} and fluoride; BeF, complex of Be^{2+} and fluoride; EPPS, *N*-2-hydroxyethylpiperazine-*N*′-3-propanesulfonic acid; $K_{0.5}$, ligand concentration giving half-maximum effect; MES, 2-[*N*-morpholino]ethanesulfonic acid; MgF, complex of Mg^{2+} and fluoride; MOPS, 3-[*N*-morpholino]propanesulfonic acid; TMAH, tetramethyl ammonium hydroxide; TNP-8N_3-ATP, 2′,3′-*O*-(2,4,6-trinitrophenyl)-8-azidoadenosine 5′-triphosphate.

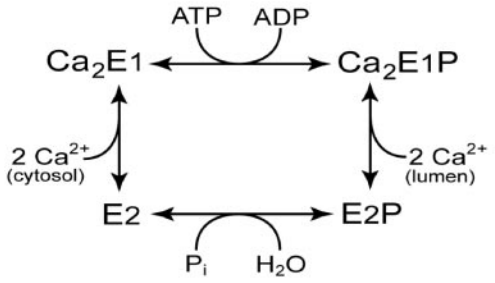

SCHEME 1. **SERCA reaction cycle.** *E*1, enzyme form with cytoplasmically facing high affinity Ca^{2+} binding sites; *E*1P, ADP-sensitive phosphoenzyme intermediate containing Ca^{2+} in the occluded state; *E*2, enzyme form with low affinity for Ca^{2+}; *E*2P, ADP-insensitive phosphoenzyme intermediate with lumenally facing low affinity Ca^{2+} binding sites.

state complex (6). Here we show that Asn^{706} likewise plays a crucial role in phosphorylation of *E*2 with P_i, as well as in the major protein conformational changes involved in phosphoenzyme and dephosphoenzyme processing. We describe here, for the first time, measurements of the apparent binding affinities of mutants for the phosphoryl analogs AlF and MgF recently used for crystallization, as well as BeF, assumed to be an analog of phosphate in the *E*2P ground state (15). These measurements suggest different roles for Asn^{706} and Glu^{183} during catalysis of the *E*2P ↔ *E*2 reaction.

EXPERIMENTAL PROCEDURES

Mutagenesis, Expression, and Assays of the Overall Reaction—Oligonucleotide-directed mutagenesis of cDNA encoding the rabbit fast-twitch muscle Ca^{2+}-ATPase (SERCA1a isoform) was carried out as described previously (16). The cDNA encoding the Ca^{2+}-ATPase mutant E183A was the same as that applied in two previous studies (10, 17). For expression, the wild-type or mutant cDNA, inserted in the pMT2 vector (18), was introduced into COS-1 cells (19) by transfection using the calcium phosphate precipitation method (20). The microsomal fraction containing expressed wild-type or mutant Ca^{2+}-ATPase was isolated by differential centrifugation (21). The concentration of expressed Ca^{2+}-ATPase was quantified by a specific enzyme-linked immunosorbent assay (22, 23). Transport of $^{45}Ca^{2+}$ into the microsomal vesicles was measured by filtration, and the ATPase activity was determined by measuring the amount of P_i liberated in the presence of ionophore A23187 to prevent inhibition caused by rebinding of Ca^{2+} to the luminally facing Ca^{2+} sites (24, 25).

Phosphorylation from [γ-^{32}*P]ATP and* $^{32}P_i$—Manual mixing experiments at various buffer and temperature conditions (detailed in the figure legends) were carried out according to the principles described previously (16, 23, 24, 26). Transient kinetic experiments at 25 °C were performed using a Bio-Logic quench-flow module QFM-5, as described (27). Acid quenching of phosphorylated enzyme was performed with 0.5–2 volumes of 25% (w/v) trichloroacetic acid containing 100 mM H_3PO_4. The acid-precipitated protein was washed by centrifugation and subjected to SDS-polyacrylamide gel electrophoresis in a 7% polyacrylamide gel at pH 6.0 (26, 28), and the radioactivity associated with the separated Ca^{2+}-ATPase band was quantified by imaging, using a Packard Cyclone™ Storage Phosphor System. Background phosphorylation levels were subtracted from all data points. The background was determined in parallel experiments, either with control microsomes isolated from mock-transfected COS-1 cells or by adding an excess of EGTA (in ATP-phosphorylation experiments) before initiating the phosphorylation. In some experiments, the constant phosphorylation level reached after an exponential decay was taken as background (usually ~5% of the initial phosphorylation).

Assays for Binding of Vanadate and Fluorides—We used the previously described assay for vanadate binding (29), and this assay, which is based on the inability of the inhibitor-bound Ca^{2+}-ATPase to be phosphorylated by ATP, was modified to study also the binding of AlF, BeF, MgF, and ADP·AlF to wild-type and mutant Ca^{2+}-pumps. Microsomes were pre-equilibrated at 25 °C and pH 7, either in the absence of Ca^{2+} to allow accumulation of the *E*2 state or in the presence of Ca^{2+} for accumulation of Ca_2E1. The reaction with inhibitor was then initiated by addition of varying concentrations of $AlCl_3$, $BeSO_4$, or $MgCl_2$ at a fixed concentration of NaF with or without ADP. In experiments involving AlF, BeF, or ADP·AlF, the concentration of Mg^{2+} (a cofactor of the reaction with the inhibitor (30–32)) was kept as low as 200 μM during the inhibition step to avoid formation of MgF. Following incubation with the inhibitor for 30 min at 25 °C and subsequent cooling for 10 min at 0 °C, the amount of inhibitor-free enzyme was determined by phosphorylation for 10 s at 0 °C with 5 μM [γ-^{32}P]ATP. In the experiments where inhibition was carried out with enzyme pre-equilibrated in the absence of Ca^{2+}, excess Ca^{2+} was added prior to the phosphorylation step (~5 s before the addition of ATP). The data presented in the supplemental material (Figs. SI and SII) validate the above described method. Fig. SI shows the time course of inhibitor binding for vanadate, AlF, BeF, MgF, and ADP·AlF. Fig. SII shows the time course of the dissociation of the enzyme·inhibitor complexes upon addition of Ca^{2+}. Note in Fig. SII that dissociation of the complexes of Ca^{2+}-ATPase with vanadate, AlF, BeF, and MgF is very slow at 0 °C, demonstrating that the 5-s incubation with Ca^{2+} prior to phosphorylation does not cause significant dissociation of enzyme·inhibitor complex. However, because the enzyme·BeF complex was more Ca^{2+}-sensitive than the complexes with AlF and MgF, we used a free Ca^{2+} concentration of only 100 μM for activation of phosphorylation in the experiments with BeF, whereas the Ca^{2+} concentration was 500 μM in the experiments with AlF and MgF.

Assays for Nucleotide Binding—The synthesis of [γ-^{32}P]TNP-8N_3-ATP, the photolabeling of COS-1 cell microsomes containing wild-type or mutant Ca^{2+}-ATPase, the inhibition of photolabeling by ATP, and the quantification of labeled bands by radioimaging following SDS-polyacrylamide gel electrophoresis were carried out as described previously (33–35).

Calculations and Data Analysis—Experiments were conducted at least twice, and the complete set of data was analyzed by nonlinear regression using the SigmaPlot program (SPSS, Inc.) or by computation using the SimZyme program (27, 36). The analysis of ligand concentration dependences was based on the Hill equation, $EP = EP_{max} \cdot [L]^n/(K^n_{0.5} + [L]^n)$, or, for the concentration dependences of inhibitory ligands, on the Hill equation for inhibition, $EP = EP_{max} \cdot (1 - [L]^n/(K^n_{0.5} + [L]^n))$. The "true" dissociation constant for ATP binding in [γ-^{32}P]TNP-8N_3-ATP labeling experiments was calculated using the validated equation for competitive inhibition (33).

RESULTS

Expression, Overall Activity, and Phosphorylation of Ca^{2+} *Pumps with Alterations to* Asn^{706}—Asn^{706} of the Ca^{2+}-ATPase was replaced by either alanine, cysteine, or serine, these mutations being chosen to either completely remove the side-chain carboxamide function (alanine) or remove the nitrogen, while retaining an oxygen in the side chain (serine), or introduce minimal negative charge (cysteine, the ionized fraction depending on the p*K* and pH), in all cases with only minor changes of the volume of the side chain. The mutant proteins were expressed in COS-1 cells, and the expression level of the mutants was similar to that obtained with wild-type Ca^{2+}-ATPase, as evaluated by

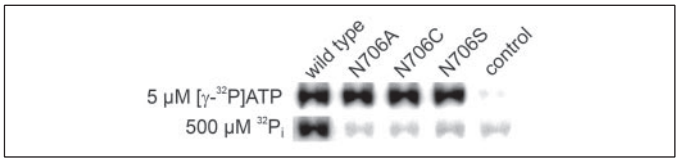

FIGURE 1. **Phosphorylation with [γ-^{32}P]ATP or $^{32}P_i$.** Phosphorylation of the microsomal preparations containing 0.5 pmol of wild-type or mutant Ca^{2+}-ATPase was carried out for 10 s at 0 °C in a buffer containing 40 mM MOPS/Tris (pH 7.0), 80 mM KCl, 5 mM $MgCl_2$, 100 μM $CaCl_2$, and 5 μM [γ-^{32}P]ATP (*upper gel*), or for 10 min at 25 °C in a buffer containing 100 mM MES/Tris (pH 6), 10 mM $MgCl_2$, 2 mM EGTA, 30% (v/v) Me_2SO, and 500 μM $^{32}P_i$ (*lower gel*), followed by acid quenching. The control corresponds to an equivalent amount (with respect to the total protein content) of microsomes harvested from mock-transfected COS-1 cells.

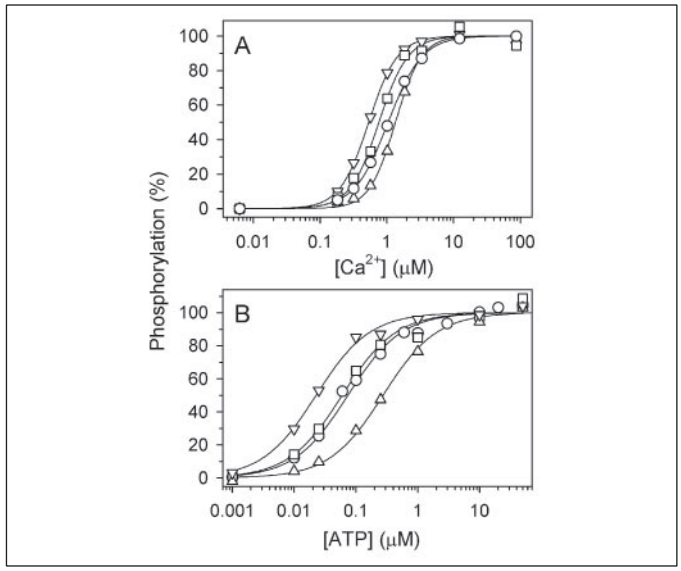

FIGURE 2. **Ca^{2+} dependence (*A*) and ATP dependence (*B*) of steady-state phosphorylation from [γ-^{32}P]ATP.** *A*, wild type and mutants were phosphorylated for 15 s at 0 °C in 40 mM MOPS/Tris (pH 7.0), 80 mM KCl, 5 mM $MgCl_2$, 1 mM EGTA, 5 μM [γ-^{32}P]ATP, and varying concentrations of $CaCl_2$ to set the free Ca^{2+} concentration as indicated. The *lines* show the best fits of the Hill equation (see "Experimental Procedures") to the data, giving the $K_{0.5}$ values indicated in parentheses: *circles*, wild type (1.05 μM); *squares*, N706A (0.76 μM); *triangles pointing upward*, N706C (1.35 μM); *triangles pointing downward*, N706S (0.54 μM). In each case, the 100% value corresponds to the phosphorylation level at infinite Ca^{2+} as deduced from the fit. *B*, phosphorylation was performed for 15 s at 0 °C in 40 mM MOPS/Tris (pH 7.0), 80 mM KCl, 5 mM $MgCl_2$, 100 μM $CaCl_2$, and varying concentrations of [γ-^{32}P]ATP as indicated. The *lines* show the best fits of the Hill equation (see "Experimental Procedures") to the data, giving the $K_{0.5}$ values indicated in parentheses: *circles*, wild type (74 nM); *squares*, N706A (60 nM); *triangles pointing upward*, N706C (274 nM); *triangles pointing downward*, N706S (23 nM). In each case, the 100% value corresponds to the phosphorylation level at infinite ATP as deduced from the fit.

their immunoreactivity in a specific enzyme-linked immunosorbent assay (data not shown). To obtain an initial overview of the functional consequences of the mutations, we measured the overall rates of $^{45}Ca^{2+}$ transport into the microsomal vesicles and ATP hydrolysis at 37 °C and saturating substrate conditions. In either assay, the three mutants displayed no significant activity above the background level obtained with control microsomes harvested from mock-transfected COS-1 cells. For N706A, the lack of ATPase activity confirms a previously published result (37).

We then proceeded to test the phosphorylation of the mutants, from [γ-^{32}P]ATP in the presence of Ca^{2+}, as well as from $^{32}P_i$ without Ca^{2+} in the backward direction of the normal reaction cycle (Scheme 1). The steady-state level of phosphoenzyme formed in the presence of 5 μM [γ-^{32}P]ATP at 0 °C was wild-type-like for all three mutants (Fig. 1, *upper gel*). However, no significant phosphoenzyme was formed in the mutants in the presence of 500 μM $^{32}P_i$ (Fig. 1, *lower gel*), under conditions where *E*2P accumulates for wild type (25 °C, presence of Me_2SO, absence of Ca^{2+}, and incubation for 10 min). Under these conditions, the concentration of P_i giving half-maximal phosphorylation of wild-type enzyme is ~10 μM, and with 500 μM P_i the reaction reaches steady-state within ~10 s (10). Thus, it is clear from Fig. 1 that the replacement of Asn^{706} affects the ability to form the *E*2P state dramatically. It should be noted that this finding is at variance with a recent study (38) reporting that mutant N706A phosphorylates with P_i to ~50% of the extent seen for wild-type Ca^{2+}-ATPase. The latter study (38) also reported 19% phosphorylation with P_i of another mutant (T353A), which we previously found unable to phosphorylate from P_i (39). We have no explanation of this apparent discrepancy. Our results were reproducible in several independent experiments carried out with different microsome preparations, and our background phosphorylation level was always rather low for mutants as well as wild-type (<5% of the maximum phosphorylation level obtained with ATP).

Ca^{2+} and MgATP Dependence of Phosphorylation from ATP—The ability of the mutants to form a phosphoenzyme from ATP allowed us to further study the partial reactions of the pump cycle in phosphorylation experiments. First, we tested the Ca^{2+} concentration dependence of steady-state phosphorylation from [γ-^{32}P]ATP (Fig. 2*A*). Small, but significant, deviations from the wild-type enzyme were found with the mutants, with the activation curve of N706S being slightly left-shifted relative to wild type and that of N706C being right-shifted. Similar effects were seen for the MgATP dependence of phosphorylation (Fig. 2*B*), corresponding to a 3-fold increase of affinity for N706S and a 4-fold reduction for N706C, relative to wild type. The observed changes of apparent affinity for Ca^{2+} as well as MgATP seem to be kinetic effects, resulting from a reduced rate of phosphoenzyme turnover in combination with various degrees of slowing of the phosphorylation rate (see below and "Discussion").

Nucleotide Binding—In a recent mutagenesis study (35) we investigated the importance of several other conserved domain P residues for the nucleotide binding properties of the Ca^{2+}-ATPase by studying the nucleotide concentration dependence of TNP-8N_3-[γ-^{32}P]ATP photolabeling and ATP/MgATP competitive inhibition thereof. Asp^{703} and Asp^{707}, which are close to Asn^{706} both in the primary and the three-dimensional structure, proved of importance for ATP/MgATP binding. Thus, charge-removal from the side chains of these aspartates enhanced ATP binding up to 14-fold in the absence of Mg^{2+}, and inhibited ATP binding up to 8-fold in the presence of Mg^{2+}. Table 1 shows the results of similar experiments carried out with the Asn^{706} mutants. It is clear that Asn^{706} is not a critical residue for TNP-8N_3-ATP or ATP binding, neither in the absence nor presence of Mg^{2+}, as the reduction of affinity was maximally 2-fold relative to wild type. It is noteworthy, however, that the largest reduction of affinity was seen in the presence of Mg^{2+} and for N706C, which also showed a significant reduction of apparent MgATP affinity in the titration of steady-state phosphorylation described above.

Time Course of ATP Phosphorylation of Ca^{2+}-saturated Enzyme—Fig. 3*A* shows the results of rapid kinetic measurements at 25 °C of the time course of phosphorylation from 5 μM MgATP of enzyme pre-equilibrated with Ca^{2+}. Compared with wild type, the phosphorylation rate was significantly reduced for N706A (1.8-fold) and N706C (4.4-fold) but unaltered for N706S (Fig. 3*A*). Because a subsaturating ATP concentration was used, the measured phosphorylation rate depends not only on the rate constant for transfer of the γ-phosphate of ATP to Asp^{351} at the catalytic site but also on the affinity of the catalytic site for ATP. Hence, at least for N706C, the slight reduction in MgATP affinity described above could contribute to determine the observed reduction of phosphorylation rate.

TABLE 1

Binding affinities for ATP and MgATP determined by inhibition of [γ-^{32}P]TNP-8N_3-ATP photolabeling

	EDTA[a]		Mg^{2+}/EGTA[b]	
	$K_{0.5}$ (TNP-8N_3-ATP)	K_D (ATP)[c]	$K_{0.5}$ (TNP-8N_3-MgATP)	K_D (MgATP)[c]
Wild type	0.19	21	0.79	0.51
N706A	0.095	17	0.72	0.74
N706C	0.12	21	1.8	0.86
N706S	0.11	16	0.99	0.55

[a] Medium: 25 mM EPPS/TMAH (pH 8.5), 20% (v/v) glycerol, 2 mM EDTA.
[b] Medium: 25 mM EPPS/TMAH (pH 8.5), 20% (v/v) glycerol, 1 mM $MgCl_2$, 0.5 mM EGTA.
[c] The "true" K_D calculated from the measured $K_{0.5}$ values under the assumption of competitive inhibition as described previously (33). In the inhibition experiments, the concentration of [γ-^{32}P]TNP-8N_3-ATP was 3× $K_{0.5}$.

Rate of the Ca^{2+}-binding Transition in the Presence or Absence of ATP—Fig. 3*B* shows the time course of phosphorylation determined under conditions similar to those corresponding to Fig. 3*A*, except that the enzyme was pre-equilibrated in the *absence* of Ca^{2+} (presence of EGTA), and phosphorylation was initiated by mixing with a buffer containing [γ-^{32}P]ATP and excess Ca^{2+}. For wild type, the rate obtained under these conditions is 1.8-fold lower than that obtained following pre-equilibration with Ca^{2+}, reflecting the rate-limiting nature of the Ca^{2+} binding transition (*i.e.* $E2 \rightarrow E1$ conformational change and accompanying Ca^{2+} binding) preceding the phosphorylation reaction (27). The three mutants displayed 4- to 6-fold lower rates of phosphorylation when starting from Ca^{2+}-deprived enzyme as compared with Ca^{2+}-pre-equilibrated enzyme (Fig. 3, compare *A* and *B*). Relative to wild type, the Ca^{2+} binding transition was 4.4-, 7.4-, and 3.2-fold slowed in N706A, N706C, and N706S, respectively (Fig. 3*B*).

In the experiment corresponding to Fig. 3*B*, 5 μM MgATP was present during the course of the Ca^{2+} binding transition. Because even micromolar concentrations of ATP accelerate $E2 \rightarrow E1$ (40), we speculated whether the inhibition of the Ca^{2+} binding transition in the Asn^{706} mutants could result from defective ATP modulation of $E2 \rightarrow E1$. We therefore examined the rate of the Ca^{2+} binding transition using an assay in which MgATP is absent during Ca^{2+} binding (Fig. 4*A*). Enzyme pre-equilibrated with EGTA was mixed with an excess amount of Ca^{2+} and incubated for varying time intervals (*t* in the mixing protocol at the *top* of Fig. 4*A*). The amount of phosphorylatable Ca_2E1 accumulated during the Ca^{2+} incubation step was then determined for each time interval by a further 34-ms incubation with 5 μM [γ-^{32}P]ATP and 5 mM Mg^{2+}, followed by acid quenching. Because the temperature and buffer conditions during the Ca^{2+} binding transition in this assay were identical to those applied in the experiment corresponding to Fig. 3*B*, except for the absence of MgATP, the rate constants obtained in the two assays can be compared directly, and their ratio reflects the modulatory influence of MgATP on the Ca^{2+} binding transition. For both wild type and mutants, the Ca^{2+} binding transition was ~2-fold slower in the absence of MgATP as compared with its presence, implying that MgATP modulation of the $E2 \rightarrow E1$ transition is unaffected by the Asn^{706} mutations. Hence, relative to wild type the Ca^{2+} binding transition in the absence of MgATP was 6.6-, 8.6-, and 4.5-fold slowed in N706A, N706C, and N706S, respectively (Fig. 4*A*).

Ca^{2+} Dissociation from the High Affinity Binding Sites in Ca_2E1—The function of the two high affinity Ca^{2+} sites in *E*1 was studied by measurement of the rate of Ca^{2+} dissociation from Ca_2E1, taking advantage of the fact that only the *E*1 form with two bound Ca^{2+} ions can be phosphorylated by ATP (41). As illustrated by the mixing protocol at the top of Fig. 4*B*, enzyme pre-equilibrated with Ca^{2+} was mixed with excess EGTA and incubated for varying time intervals. The amount of phosphorylatable Ca_2E1 remaining after the EGTA incubation step was then determined for each time interval by a further 34-ms incubation with 5 μM [γ-^{32}P]MgATP, followed by acid

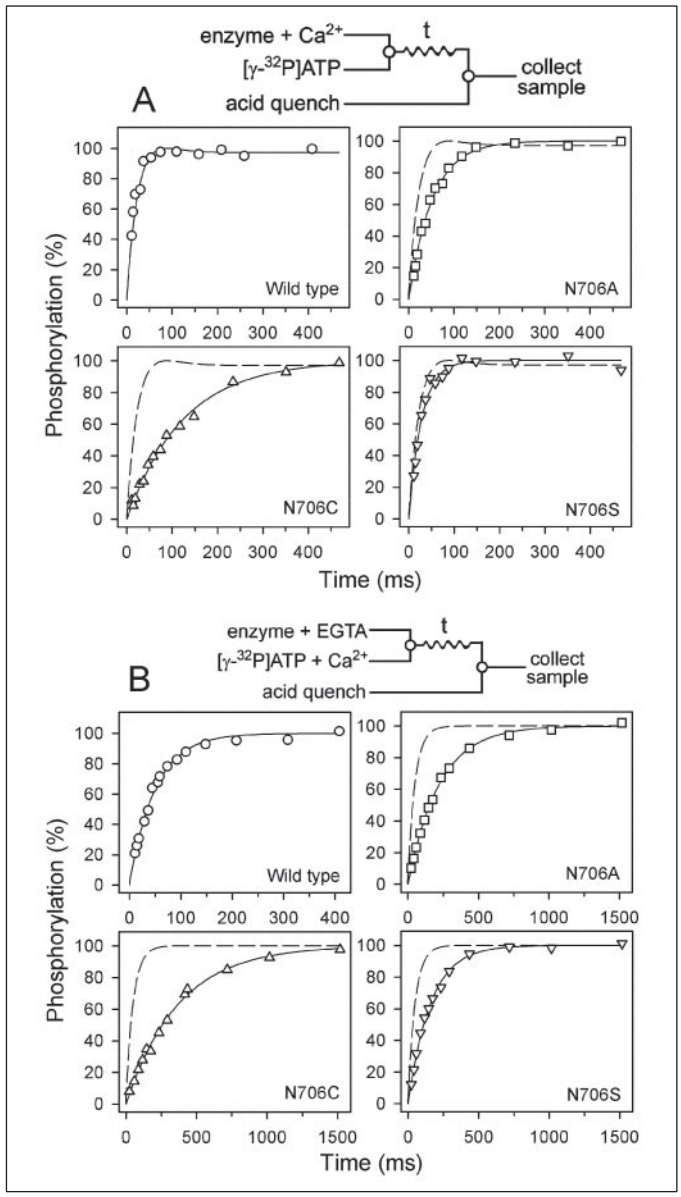

FIGURE 3. **Rapid kinetics of phosphorylation from [γ-^{32}P]ATP of enzyme pre-equilibrated with (*A*) or without (*B*) Ca^{2+}.** Quench-flow experiments were carried out using a QFM-5 quench-flow module at 25 °C with mixing protocols as illustrated above the panels. *A*, to monitor the phosphorylation of enzyme initially present in the Ca^{2+}-bound state, microsomes suspended in a buffer containing 40 mM MOPS/Tris (pH 7.0), 80 mM KCl, 5 mM $MgCl_2$, and 100 μM $CaCl_2$ were mixed with an equal amount of the same buffer containing in addition 10 μM [γ-^{32}P]ATP, followed by acid quenching at the indicated time intervals. The *lines* show the results of computations carried out as previously described using the SimZyme program (27, 36) with the following rate constants for the $Ca_2E1 \rightarrow Ca_2E1P$ reaction step: wild type, 35 s^{-1}; N706A, 19 s^{-1}; N706C, 8 s^{-1}; N706S, 35 s^{-1}. The *broken lines* correspond to the wild-type curve from the *upper left panel*. In each case, the maximal level of phosphorylation was taken as 100%. *B*, to monitor the phosphorylation of enzyme initially present in the Ca^{2+}-deprived state, microsomes suspended in a buffer containing 40 mM MOPS/Tris (pH 7.0), 80 mM KCl, and 2 mM EGTA were mixed with an equal amount of a buffer containing 40 mM MOPS/Tris (pH 7.0), 80 mM KCl, 10 mM $MgCl_2$, 2.2 mM $CaCl_2$, and 10 μM [γ-^{32}P]ATP, followed by acid quenching at the indicated time intervals. The *lines* show the best fits of a monoexponential function giving the following rate constants: wild type, 20 s^{-1}; N706A, 4.5 s^{-1}; N706C, 2.7 s^{-1}; N706S, 6.3 s^{-1}. The *broken lines* correspond to the wild-type curve from the *upper left panel*. In each case, the 100% value corresponds to the phosphorylation level at infinite time as deduced from the fit.

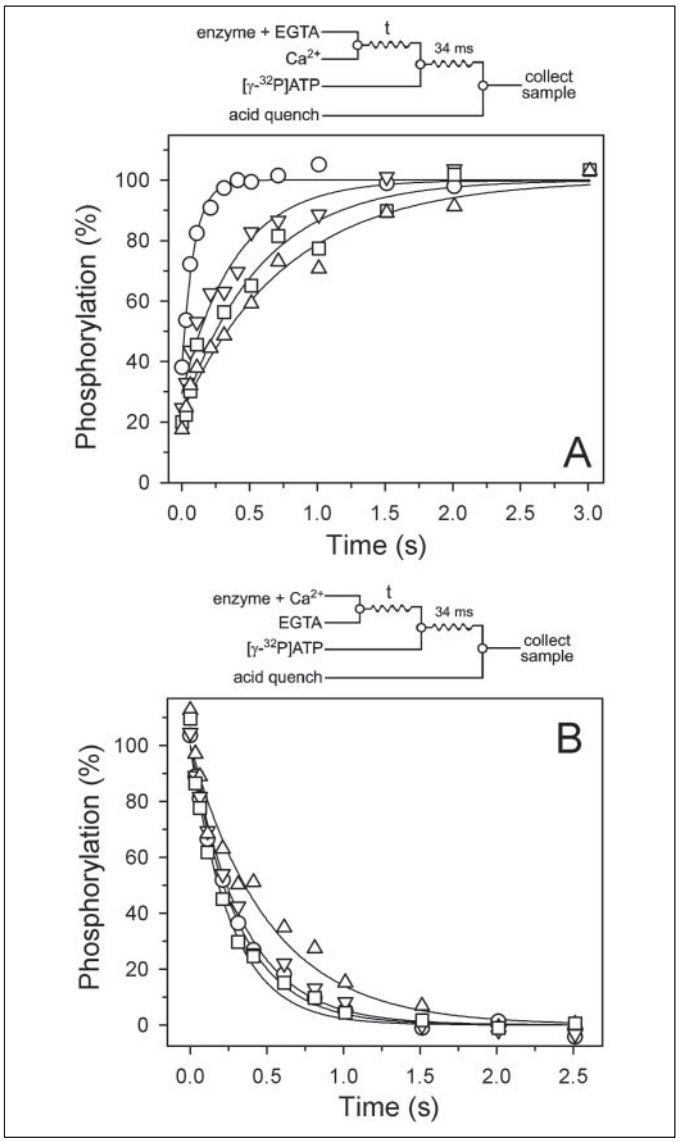

FIGURE 4. **Kinetics of Ca^{2+} binding (*A*) and Ca^{2+} dissociation (*B*).** *A*, time course of the Ca^{2+} binding transition determined by measuring the appearance of ability to phosphorylate. Quench-flow experiments were carried out as illustrated by the diagram above the panel using a QFM-5 module at 25 °C. Wild-type or mutant enzyme, preincubated in 40 mM MOPS/Tris (pH 7.0), 80 mM KCl, and 2 mM EGTA, was mixed with an equal volume of 40 mM MOPS/Tris (pH 7.0), 80 mM KCl, and 2.2 mM $CaCl_2$. At the indicated time intervals, the double volume of 40 mM MOPS/Tris (pH 7.0), 80 mM KCl, 10 mM $MgCl_2$, 1 mM EGTA, 10 μM [γ-^{32}P]ATP, and 1.1 mM $CaCl_2$ was added, followed by acid quenching 34 ms later. To obtain the point corresponding to zero time, the enzyme was preincubated in a buffer containing 40 mM MOPS/Tris (pH 7.0), 80 mM KCl, and 2 mM EGTA, and mixed with an equal volume of 40 mM MOPS/Tris (pH 7.0), 80 mM KCl, 10 mM $MgCl_2$, 10 μM [γ-^{32}P]ATP, and 2.2 mM $CaCl_2$, followed by acid quenching 34 ms later. The *lines* show the best fits of a monoexponential function with an initial offset, giving the rate constants indicated in parentheses: *circles*, wild type (11.2 s^{-1}); *squares*, N706A (1.7 s^{-1}); *triangles pointing upward*, N706C (1.3 s^{-1}); *triangles pointing downward*, N706S (2.5 s^{-1}). In each case, the 100% value corresponds to the phosphorylation level at infinite time as deduced from the fit. *B*, time course Ca^{2+} dissociation from the high affinity sites toward the cytoplasm determined by measuring the disappearance of ability to phosphorylate. Quench-flow experiments were carried out as illustrated by the diagram above the panels using a QFM-5 module at 25 °C. Wild-type or mutant enzyme, preincubated in 40 mM MES/Tris (pH 6.0), 80 mM KCl, 5 mM $MgCl_2$, and 100 μM $CaCl_2$, was mixed with an equal volume of 40 mM MES/Tris (pH 6.0), 80 mM KCl, 5 mM $MgCl_2$, and 4 mM EGTA. At the indicated time intervals, the double volume of 40 mM MES/Tris (pH 6.0), 80 mM KCl, 5 mM $MgCl_2$, 2 mM EGTA, and 10 μM [γ-^{32}P]ATP was added, followed by acid quenching 34 ms later. To obtain the point corresponding to zero time, 4 mM EGTA was replaced by 100 μM $CaCl_2$. The *lines* show the best fit of a monoexponential decay function, giving the rate constants indicated in parentheses: *circles*, wild type (3.2 s^{-1}); *squares*, N706A (3.8 s^{-1}); *triangles pointing upward*, N706C (2.0 s^{-1}); *triangles pointing downward*, N706S (2.9 s^{-1}). In each case, the phosphorylation level corresponding to zero time was taken as 100%.

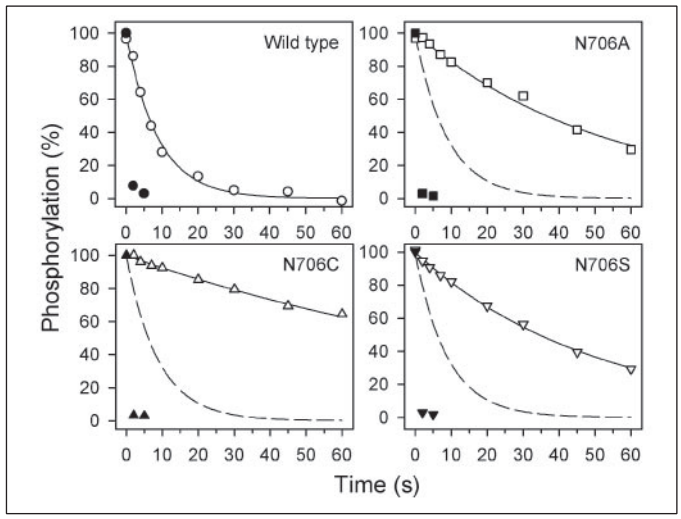

FIGURE 5. **Dephosphorylation of phosphoenzyme formed from [γ-^{32}P]ATP.** Wild-type or mutant enzyme was phosphorylated for 15 s at 0 °C in a buffer containing 40 mM MOPS/Tris (pH 7.0), 80 mM KCl, 5 mM $MgCl_2$, 1 mM EGTA, 0.955 mM $CaCl_2$ (giving a free Ca^{2+} concentration during phosphorylation of 10 μM), 2 μM calcium ionophore A23187, and 5 μM [γ-^{32}P]ATP. To measure dephosphorylation, the phosphoenzyme was chased at 0 °C by addition of 10 mM EGTA to remove Ca^{2+}, either without (*open symbols*) or with (*solid symbols*) 1 mM ADP, and acid quenching was performed at the indicated time intervals. The *lines* show the best fits of a monoexponential decay function, giving the rate constants indicated in parentheses: *open circles*, wild type (0.113 s^{-1}); *open squares*, N706A (0.019 s^{-1}); *open triangles pointing upward*, N706C (0.0078 s^{-1}); *open triangles pointing downward*, N706S (0.020 s^{-1}). The *broken lines* correspond to the wild-type curve from the *upper left panel*. In each case, the phosphorylation level at zero time was taken as 100%.

quenching. Because only the Ca^{2+}-bound enzyme fraction phosphorylates, the rate of disappearance of ability to phosphorylate reflects the rate of Ca^{2+} dissociation. As seen in Fig. 4*B*, there were only minor differences between the Ca^{2+} dissociation rates of the wild-type and the Asn^{706} mutants, apparently excluding a role for Asn^{706} in Ca^{2+} binding or in the conformational changes involved in Ca^{2+} dissociation from the high affinity sites.

The $Ca_2E1P \rightarrow E2P$ Conformational Transition of the Phosphoenzyme—To investigate the processing of the phosphoenzyme, the enzyme was phosphorylated with [γ-^{32}P]ATP under conditions where Ca_2E1P accumulates as the major steady-state intermediate in the wild-type enzyme (0 °C, presence of K^+, neutral pH). Phosphoenzyme decay in the forward direction of the pump cycle was examined by addition of excess EGTA to terminate phosphorylation by removing Ca^{2+}, followed by acid quenching at varying time intervals. As shown in Fig. 5 (*open symbols*), all three mutants displayed reduced rates of phosphoenzyme turnover relative to wild type (2.4-, 8.8-, and 2.9-fold for N706A, N706C, and N706S, respectively). For wild type, the conformational change of the phosphoenzyme, the $Ca_2E1P \rightarrow E2P$ transition, is rate-limiting for the overall ATPase reaction, whereas the ensuing dephosphorylation of *E*2P (*cf.* Scheme 1) is much faster in the presence of K^+ at neutral pH. The Ca_2E1P state is characterized by being able to donate its phosphoryl group back to ADP, forming ATP, whereas *E*2P is ADP insensitive and dephosphorylates only by hydrolysis of the acyl phosphate. To determine whether the $Ca_2E1P \rightarrow E2P$ step or $E2P \rightarrow E2$ is rate-limiting in the mutants, we measured the ADP sensitivity of the accumulated phosphoenzyme. The dephosphorylation solution was supplemented with 1 mM ADP, and phosphoenzyme decay was again followed (Fig. 5, *solid symbols*). For the three mutants, as well as the wild type, all phosphoenzyme disappeared completely within 5 s of the addition of ADP, demonstrating that the accumulated phosphoenzyme was entirely ADP-sensitive Ca_2E1P. Similar experiments were carried out under buffer conditions where a high level of *E*2P accumulates at steady state in wild type (pH 8 and K^+

replaced by Li^+, *cf.* Ref. 10), and again no significant level of *E*2P was detected in the Asn^{706} mutants (data not shown). The fact that no ADP-insensitive *E*2P had accumulated shows that the low rate of phosphoenzyme processing in the mutants, corresponding to the *open symbols* in Fig. 5, results from a block of the $Ca_2E1P \rightarrow E2P$ transition, and that *E*2P hydrolysis is not grossly slowed in the mutants.

Affinity of E2 for Vanadate—As demonstrated above (Fig. 1), none of the Asn^{706} mutants showed any phosphorylation from inorganic phosphate, even after incubation for a long time at a concentration of P_i 50-fold higher than the concentration required for half-maximal phosphorylation of wild type. Because the mutants could easily undergo phosphorylation from ATP, the binding of the phosphate analog vanadate could be examined by taking advantage of the competition between ATP and vanadate, as previously described (29). Vanadate, which often is considered to mimic a penta-coordinated transition state of the phosphoryl group, binds to *E*2 in a slow reaction that requires Mg^{2+} (42, 43). Ca^{2+}-deprived enzyme was equilibrated at 25 °C with varying concentrations of vanadate in the presence of Mg^{2+}, and the level of vanadate-free enzyme was determined for each vanadate concentration after cooling to 0 °C (to slow vanadate dissociation as much as possible), by measuring the phosphorylation level obtained upon addition of excess Ca^{2+} and [γ-^{32}P]ATP. As seen in Fig. 6, the wild-type enzyme displayed half-maximal inhibition of phosphorylation at 0.16 μM vanadate. In contrast, the three mutants with alterations to Asn^{706} displayed $K_{0.5}$ values at least three orders of magnitude higher than that of wild type (Fig. 6 and Table 2). A similar insensitivity to inhibition by vanadate was previously described for a mutant in which Glu^{183} in domain A had been replaced by alanine (Ref. 10; for comparison the previously reported data for E183A is included in Fig. 6 and Table 2). However, the E183A mutant differed from the mutants with alterations to Asn^{706} by being able to slowly form *E*2P from P_i, *i.e.* the rate of catalysis was more strongly affected than the stability of *E*2P in this case. For further comparison, the E183A mutant was included in the experiments described below.

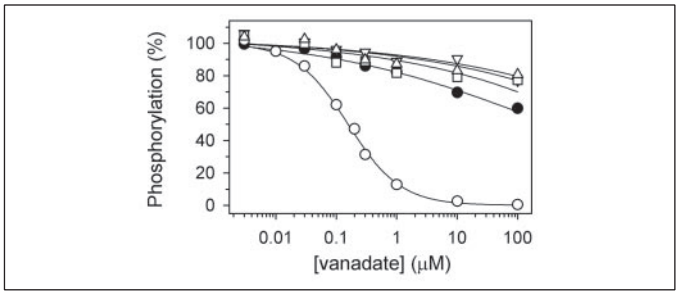

FIGURE 6. **Vanadate binding to *E*2 determined by inhibition of phosphorylation from [γ-^{32}P]ATP.** Microsomes were incubated for 1 h at 25 °C and subsequently 15 min at 0 °C in a buffer containing 40 mM MOPS/Tris (pH 7.0), 80 mM KCl, 2 mM EGTA, 5 mM $MgCl_2$, and the indicated concentration of orthovanadate. The level of inhibition was then tested at 0 °C by sequential addition of 2.5 mM $CaCl_2$ and 5 μM [γ-^{32}P]ATP, followed by acid quenching 15 s later. The maximum level of phosphorylation obtained in the absence of vanadate was taken as 100%. The *lines* show the best fit of the Hill equation for inhibition (see "Experimental Procedures") to the data, giving the $K_{0.5}$ values indicated in parentheses: *open circles*, wild type (0.16 μM); *squares*, N706A (>100 μM); *triangles pointing upward*, N706C (>100 μM); *triangles pointing downward*, N706S (>100 μM); *solid circles*, E183A (>100 μM).

Affinity of E2 for the Phosphate Analogs AlF, BeF, and MgF—Like vanadate, the complexes of Al^{3+}, Be^{2+}, and Mg^{2+} with fluoride are considered phosphate analogs that bind to the Ca^{2+}-deprived *E*2 state of Ca^{2+}-ATPase (15, 30–32). Most likely, the bound fluoride complexes are AlF_4^- or AlF_3, MgF_4^{2-}, and BeF_3^- (6, 7, 15), but due to the uncertainty about the actual number of fluoride atoms in the bound complexes, they will here be denoted simply AlF, BeF, and MgF. Danko *et al.* (15) compared the properties of the phosphorylated enzyme with those of the *E*2·vanadate, *E*2·AlF, *E*2·BeF, and *E*2·MgF complexes, using limited proteolysis as well as trinitrophenyl-AMP and intrinsic tryptophan fluorescence analysis, and came to the conclusion that the *E*2·BeF form is similar to the *E*2P ground state with covalently bound phosphate but distinct from *E*2·vanadate, *E*2·AlF, and *E*2·MgF forms. The BeF complex would thus be BeF_3^-, adopting a tetrahedral geometry with the fourth coordination from the oxygen atom of Asp^{351} (see Table 2). In light of the arrangements of AlF and MgF in crystal structures of other phosphotransferases, the *E*2·AlF form was suggested to represent the transition state occurring during *E*2P hydrolysis, either as AlF_4^- or as AlF_3 (in both cases with planar geometry), with two oxygen atoms coordinating to the aluminum at apical positions to produce a state superposable (AlF_3) or analogous (AlF_4^-) to the trigonal bipyramidal structure of the penta-coordinated phosphorous in the transition state of an in-line associative acylphosphate hydrolysis mechanism. The *E*2·MgF form was, on the other hand, suggested to mimic the product state of *E*2P hydrolysis (*E*2·P_i) with the non-covalently bound P_i being represented by MgF_4^{2-} of tetrahedral geometry (15), see Table 2. The recently published crystal structures of Ca^{2+}-

TABLE 2

Summary of vanadate, BeF, AlF, and MgF binding to *E*2 and ADP·AlF binding to Ca_2E1

$K_{0.5}$ values for inhibition are displayed relative to the values obtained with wild type (the original $K_{0.5}$ values are listed in the legends to Figs. 6–8). For MgF, the values in parentheses refer to the experiments where the Mg^{2+} concentration was kept constant and the fluoride concentration varied.

Enzyme state		*E*2				Ca_2E1
Inhibitor		Vanadate Fig. 6	BeF Fig. 7*B*	AlF Fig. 7*A*	MgF Fig. 7*C* (Fig. 7*D*)	ADP·AlF Fig. 8
Presumed state of phosphate represented by inhibitor			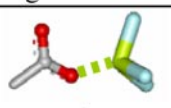 *ground state*	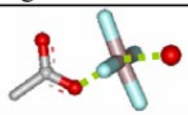 *transition state*	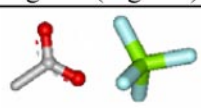 *product state*	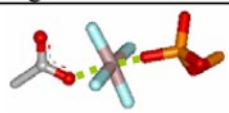 *transition state*
Mutant	**Wild type**	1	1	1	1 (1)	1
	N706A	>1000	15	2.9	16 (7.4)	4.1
	N706C	>1000	32	3.5	8.3 (3.9)	15
	N706S	>1000	6.1	1.2	1.9 (1.5)	1.6
	E183A	>1000	9.3	16	4.1 (2.7)	1.8

ATPase in *E*2 with bound AlF or MgF (6, 7) seem to confirm the proposals by Danko *et al.* (15) with respect to the structure of the bound AlF and MgF complexes, whereas no crystal structure of Ca^{2+}-ATPase with bound BeF has yet been solved. Thus, the structure analogous to genuine *E*2P is still missing. The distinctions are important for the pumping mechanism, because the AlF and MgF protein complexes do not have an obvious passage for Ca^{2+} access from the lumen, whereas such a passage may exist in *E*2·BeF and *E*2P (15).

To obtain more detailed information about the roles of Asn^{706} and Glu^{183} in interaction with the phosphoryl group in various *E*2 states, and to learn more about the differential characteristics of the fluoride complexes and vanadate, we studied the binding of AlF (Fig. 7*A*), BeF (Fig. 7*B*), and MgF (Fig. 7, *C* and *D*) to wild type and mutants, using the same method as described above for vanadate, which takes advantage of the competition at the catalytic site. This was feasible, because these phosphate analogs, like vanadate, all dissociate slowly from the Ca^{2+}-ATPase (BeF was found to dissociate at approximately the same rate as vanadate under the conditions applied, and AlF and MgF dissociated even slower, see Fig. SII in supplemental materials). To study AlF binding, Ca^{2+}-deprived enzyme was incubated for 30 min at 25 °C with 2 mM NaF, 200 μM Mg^{2+}, and varying concentrations of $AlCl_3$, followed by cooling on ice. Mg^{2+} at low concentration is required for the formation of the enzyme complex with AlF, but only 200 μM was added during the AlF binding step to avoid formation of MgF, *cf.* Fig. 7 (*C* and *D*). The uncomplexed fraction of the enzyme was then determined by measuring the phosphorylation occurring during a 10-s incubation with 5 μM [γ-^{32}P]ATP at 0 °C after supplementing the medium with excess Ca^{2+} and 5 mM Mg^{2+}. Wild-type Ca^{2+}-ATPase displayed half-maximal inhibition of phosphorylation at 8.8 μM $AlCl_3$ (Fig. 7*A*). In control experiments where no NaF had been added, >200 μM $AlCl_3$ (probably binding at Ca^{2+} sites) was required to obtain half-maximal inhibition (*broken line* in Fig. 7*A*; data points shown only for wild type, but identical data were obtained for the mutants). The mutants with alterations to Asn^{706} were also very sensitive to inhibition by AlF, contrasting their lack of sensitivity to vanadate (*cf.* Fig. 6). Thus, the AlF inhibition profile of N706S was indistinguishable from that of the wild type, and N706A and N706C displayed ~3-fold reduced apparent affinities for AlF, relative to wild type (Fig. 7*A* and Table 2). E183A, on the other hand, displayed very low AlF affinity (16-fold reduced relative to wild type). In fact, there was little difference between the result of the AlF titration experiment with E183A and the control experiment, where Al^{3+} was added in the absence of NaF.

We then proceeded to study the binding of BeF to *E*2 (Fig. 7*B* and Table 2). The assay was carried out as described above for AlF, except that $AlCl_3$ was replaced by $BeSO_4$. Wild-type Ca^{2+}-ATPase displayed half-maximal inactivation at 0.8 μM $BeSO_4$, *i.e.* 11-fold higher apparent affinity than with $AlCl_3$. The effects of the Asn^{706} mutations on BeF binding were markedly stronger than the effects on AlF binding. Thus, N706C displayed a 32-fold reduced affinity for BeF relative to wild type (compare with the 3.5-fold reduced affinity of N706C for AlF). A similar pattern was seen for N706A and N706S (15- and 6.1-fold reduced affinities for BeF, respectively, compare with the respective 2.9-fold reduced and wild type-like affinities for AlF). E183A was rather similar to the Asn^{706} mutants with respect to BeF binding, displaying 9.3-fold reduced affinity for BeF relative to wild type. As was the case with Al^{3+}, Be^{2+} in the absence of NaF also inhibited the enzyme at high concentrations (*broken line* in Fig. 7*B*; data points only shown for wild type, but identical data were obtained for the mutants).

The binding of MgF to *E*2 was likewise examined (Fig. 7, *C* and *D*, and Table 2). The results shown in Fig. 7*C* were obtained as described above for AlF, except that $AlCl_3$ was replaced by $MgCl_2$ (and Mg^{2+} thus excluded from the standard reaction buffer), and that 5 mM NaF was used instead of 2 mM to increase the amount of MgF formed as much as possible (the formation constant for MgF is considerably lower that those pertaining to AlF and BeF (44), with resulting lower expected

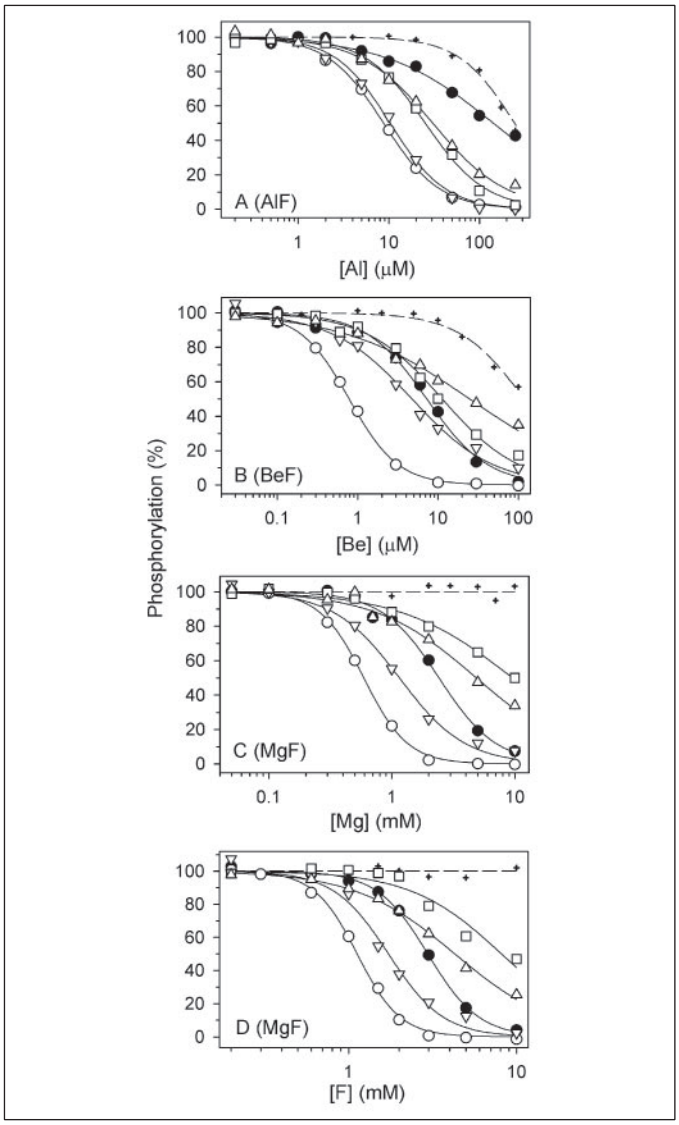

FIGURE 7. **AlF, BeF, and MgF binding to *E*2 determined by inhibition of phosphorylation from [γ-^{32}P]ATP.** Microsomes were incubated for 30 min at 25 °C and subsequently 10 min at 0 °C in buffers containing 40 mM MOPS/Tris (pH 7.0), 80 mM KCl, 2 mM EGTA, and 200 μM $MgCl_2$, 2 mM NaF, and the indicated concentrations of $AlCl_3$ (*A*), 200 μM $MgCl_2$, 2 mM NaF, and the indicated concentrations of $BeSO_4$ (*B*), 5 mM NaF and the indicated concentrations of $MgCl_2$ (*C*), or 5 mM $MgCl_2$ and the indicated concentrations of NaF (*D*). The level of inhibition was then tested at 0 °C by sequential addition of 2.5 mM $CaCl_2$ and 5 μM [γ-^{32}P]ATP with 5 mM $MgCl_2$ (*A* and *C*), 2.1 mM $CaCl_2$ and 5 μM [γ-^{32}P]ATP with 5 mM $MgCl_2$ (*B*), or 2.5 mM $CaCl_2$ and 5 μM [γ-^{32}P]ATP (*D*), followed by acid quenching 10 s later. In each case, the maximum level of phosphorylation was taken as 100%. [γ-^{32}P]ATP was added as quickly as possible (~5 s) after the addition of $CaCl_2$ to avoid Ca^{2+}-induced dissociation of the enzyme·inhibitor complex (*cf.* Fig. SII in the supplemental material). *Open circles*, wild type; *squares*, N706A; *triangles pointing upward*, N706C; *triangles pointing downward*, N706S; *solid circles*, E183A. The data points represented by a *broken line with crosshair symbols* correspond to control experiments in which either NaF (*A–C*) or Mg^{2+} (*D*) was excluded from the reaction buffer (data points only shown for wild type, but none of the mutants deviated significantly from the wild type in this respect). The *lines* show the best fits to the data of an arbitrary Hill equation for inhibition (see "Experimental Procedures"), giving the following $K_{0.5}$ values: *A* (Al^{3+} titration at 2 mM NaF): wild type, 8.8 μM; N706A, 25 μM; N706C, 31 μM; N706S, 10.4 μM; E183A, 143 μM; wild-type control without NaF, 245 μM; *B* (Be^{2+} titration at 2 mM NaF): wild type, 0.78 μM; N706A, 11 μM; N706C, 25 μM; N706S, 4.8 μM; E183A, 7.3 μM; wild-type control without NaF (119 μM); *C* (Mg^{2+} titration at 5 mM NaF): wild type, 0.59 mM; N706A, 9.6 mM; N706C, 4.9 mM; N706S, 1.15 mM; E183A, 2.4 mM; wild-type control without NaF, no inhibition up to 10 mM Mg^{2+}; and *D* (NaF titration at 5 mM Mg^{2+}): wild type, 1.1 mM; N706A, 8.1 mM; N706C, 4.3 mM; N706S, 1.7 mM; E183A, 3.0 mM; wild-type control without Mg^{2+}, no inhibition up to 10 mM NaF.

apparent affinity for MgF as compared with the other fluoride complexes). In Fig. 7*D*, the roles of NaF and $MgCl_2$ were reversed: the added $MgCl_2$ concentration being kept constant at 5 mM while the added NaF concentration was varied (note the *broken line*, demonstrating that fluoride alone at concentrations up to 10 mM is without effect, this also serves as fluoride control in the other experiments). Irrespective of whether $MgCl_2$ or NaF was varied, the results looked the same, consistent with the idea that the inhibitory compound is a complex between Mg^{2+} and F^- and not any of these species in their uncomplexed state. All four mutants displayed significant affinity shifts relative to wild type, with N706A and N706C showing the most marked effects (7.4- to 16-fold and 3.9- to 8.3-fold reduction of apparent affinity, respectively), N706S (1.5- to 1.9-fold reduction of apparent affinity) being only slightly less sensitive to MgF inhibition than wild type, and E183A displaying an intermediate behavior (2.7- to 4.1-fold reduction of apparent affinity).

Affinity of Ca$_2$E1 for ADP·AlF—ADP and AlF bind together with high affinity in a complex with the Ca_2E1 state of wild-type Ca^{2+}-ATPase, with concomitant tight occlusion of the two Ca^{2+} ions at the transport sites (31). Because the Ca_2E1 enzyme complex with ADP·AlF is believed to mimic the transition state in the transfer of the γ-phosphoryl group from ATP (5, 7), we also studied the effects of the Asn^{706} and Glu^{183} mutations on formation of this complex, using the same assay as described above, but including 100 μM Ca^{2+} and 1 μM ADP during complex formation (Fig. 8). The presence of Ca^{2+} ensures that the enzyme is in Ca_2E1. Hence, the E_2 conformation reacting with AlF in the absence of ADP (*cf.* Fig. 7*A*) is depleted (as illustrated by the *broken line* in Fig. 8, inhibition by AlF is rather weak in the absence of ADP when Ca^{2+} is present). The ADP concentration of 1 μM was chosen as a compromise, being sufficient to cause marked inhibition of wild-type Ca^{2+}-ATPase in the presence of $AlCl_3$ and NaF, without interfering significantly with the phosphorylation of uncomplexed enzyme from MgATP (data not shown). Fig. 8 shows that the wild type displayed a $K_{0.5}$ of 3.7 μM for inhibition under these conditions. N706A and N706C displayed markedly increased $K_{0.5}$ values (reduced apparent affinities) relative to wild type (4.1- and 15-fold, respectively, see Table 2), whereas N706S differed only slightly from wild type. E183A likewise displayed only 1.8-fold reduced apparent affinity for ADP·AlF relative to wild type (Fig. 8 and Table 2).

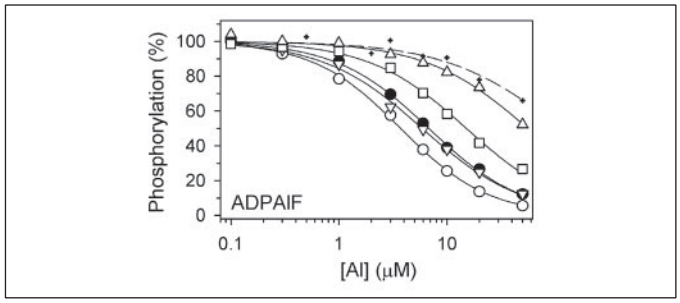

FIGURE 8. **ADP·AlF binding to Ca_2E1 determined by inhibition of phosphorylation from [γ-^{32}P]ATP.** Microsomes were incubated for 30 min at 25 °C followed by 10 min at 0 °C in a buffer containing 40 mM MOPS/Tris (pH 7.0), 80 mM KCl, 200 μM $MgCl_2$, 100 μM $CaCl_2$, 2 mM NaF, 1 μM ADP, and varying concentrations of $AlCl_3$ as indicated. The level of inhibition was then tested at 0 °C by addition of 5 μM [γ-^{32}P]ATP with 5 mM $MgCl_2$, followed by acid quenching 10 s later. The level of phosphorylation obtained in the absence of $AlCl_3$ was taken as 100%. The data points represented by a *broken line with crosshair symbols* correspond to a control experiment in which ADP was excluded from the reaction buffer (data points only shown for wild type, but none of the mutants deviated significantly from wild type in this respect). The *lines* show the best fits of the Hill equation for inhibition (see "Experimental Procedures") to the data, giving the $K_{0.5}$ values indicated in parentheses: *open circles*, wild type (3.7 μM); *squares*, N706A (15 μM); *triangles pointing upward*, N706C (56 μM); *triangles pointing downward*, N706S (5.9 μM); *solid circles*, E183A (6.8 μM); *crosshair symbols*, wild-type control without ADP (113 μM).

DISCUSSION

In this study, we have explored the functional consequences of mutations of Asn^{706} in domain P of Ca^{2+}-ATPase. It is informative to analyze the results obtained with the Asn^{706} mutants in relation to the crystal structures of the Ca^{2+}-ATPase (Fig. 9), and furthermore to compare with the results obtained previously (10), and in the present study, with mutant E183A, where the glutamate of the conserved TGES motif of domain A is replaced. Mutations of Asn^{706} and Glu^{183} have in common that they dramatically impede the function of the enzyme in *E*2 forms, but have less striking effects on *E*1. In our previous study (10), we showed that replacement of Glu^{183} with alanine leads to a reduced rate of both *E*2P dephosphorylation and the reverse phosphorylation of *E*2 with P_i, suggesting that Glu^{183} is very critical for catalysis and, thus, for transition state stabilization. The functional analysis turned out to correlate well with the location of Glu^{183} in the subsequently published *E*2·AlF crystal structure (Fig. 9). In this structure, the AlF complex

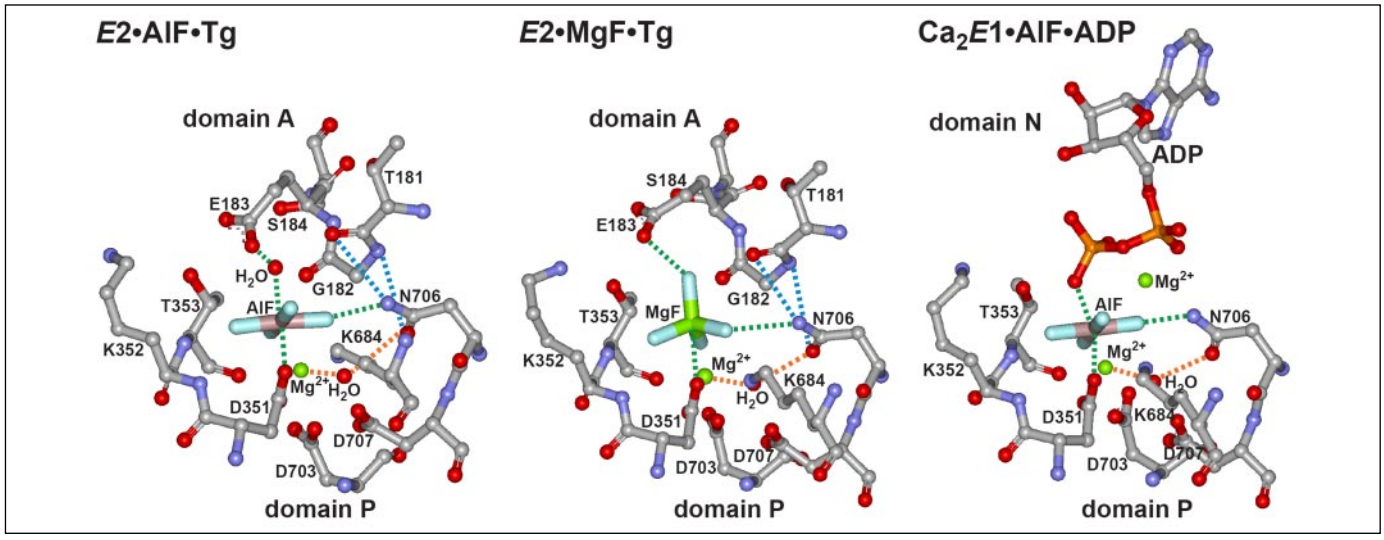

FIGURE 9. **Structural organization of the catalytic site of Ca^{2+}-ATPase crystallized in the *E*2·AlF state, the *E*2·MgF state, and the Ca_2E1·AlF·ADP state.** Views of the catalytic site in the crystal structures of the thapsigargin-stabilized *E*2·AlF and *E*2·MgF states and the Ca_2E1·AlF·ADP state of Ca^{2+}-ATPase (Protein Data Bank accession codes 1XP5 (6), 1WPE (7), and 1T5T (5), respectively). Carbon and aluminum atoms are shown in *gray*, nitrogen in *blue*, oxygen in *red*, phosphorus in *orange*, magnesium in *green*, and fluoride in *cyan*. The interactions discussed are indicated by *green*, *blue*, and *orange broken lines*, as specified in the text.

(modeled as AlF_4^-) is planar and is positioned linearly between one of the carboxylate oxygens of Asp^{351} and a water molecule, held and likely activated by Glu^{183} for nucleophilic attack on the phosphorous atom (6). It is clear from the present results that Asn^{706} is also a critical residue for *E*2P formation. However, whereas for mutant E183A *E*2P phosphoenzyme formed from P_i *did*, in fact, accumulate (though slowly relative to wild type), none of the mutants with alterations to Asn^{706} showed any accumulation of *E*2P, even after incubation for a long time at a concentration of P_i 50-fold higher than the concentration required for half-maximal phosphorylation of wild type (Fig. 1). The lack of ability to phosphorylate from P_i prevented us from studying the rate of *E*2P hydrolysis directly in the Asn^{706} mutants, but some of the data obtained with the phosphoenzyme formed from ATP suggest that the *E*2P hydrolysis step is not as inhibited in these mutants as it is in E183A. Asn^{706} therefore seems to play a less critical role than Glu^{183} in stabilization of the transition state in *E*2P hydrolysis. Thus, virtually all phosphoenzyme accumulated at steady state following reaction of the three Asn^{706} mutants with ATP was ADP-sensitive Ca_2E1P (Fig. 5). In comparison, 43% of the phosphoenzyme accumulated under identical conditions with E183A was ADP-insensitive *E*2P, despite a reduced rate of the $Ca_2E1P \rightarrow E2P$ transition in E183A (10), thus reflecting the reduced rate of *E*2P hydrolysis in the latter mutant. Even in phosphorylation experiments with ATP carried out under buffer conditions where a high level of *E*2P accumulates at steady state in wild type (*i.e.* pH 8 and K^+ replaced by Li^+), no significant level of *E*2P accumulated in the mutants with alterations to Asn^{706}. Thus, unlike E183A, the mutations of Asn^{706} do not seem to impair *E*2P hydrolysis markedly; in fact it may even be enhanced, due to destabilization of *E*2P.

Danko *et al.* (15) proposed a distinction between *E*2·BeF, *E*2·AlF, and *E*2·MgF as analogs of the ground state, transition state, and *E*2·P_i product state, respectively, in *E*2P hydrolysis. In contrast to the planar tetragonal AlF complex of the *E*2·AlF crystal structure, that seems to mimic the transition state of *E*2P hydrolysis, the MgF complex (*i.e.* MgF_4^{2-}) is in a tetrahedral arrangement in the *E*2·MgF crystal structure (see Fig. 9 and Table 2), implying that *E*2·MgF represents the *E*2·P_i product state of *E*2P hydrolysis. The *E*2·BeF complex (of which no crystal structure has yet been published) shares several features with the *E*2P ground state, including an increased hydrophobicity of the nucleotide site relative to *E*2, *E*2·AlF, *E*2·MgF, and *E*2·vanadate. Furthermore, *E*2·BeF displays a high sensitivity to luminal Ca^{2+} (a feature not seen with *E*2·AlF and *E*2·MgF), as one would expect from a true *E*2P ground state with luminally exposed Ca^{2+} sites (15). With respect to BeF binding (Fig. 7*B*), all four mutants displayed significant shifts toward lower apparent affinity relative to wild type (6- to 32-fold), suggesting that both Asn^{706} and Glu^{183} contribute significantly to stabilization of the *E*2P ground state. The affinities for AlF and MgF differed more significantly among the four mutants. The affinity for AlF (Fig. 7*A*) was markedly reduced in E183A relative to wild type, consistent with Glu^{183} being involved in stabilization of the *E*2P transition state. The affinity for AlF was much less affected in the mutants with alterations to Asn^{706} than in E183A, N706S, in particular, being completely wild type-like (Fig. 7*A*), thus suggesting that the side chain of Asn^{706} contributes marginally or not at all to the stability of the *E*2P transition state, in line with the results of studies of the phosphoenzyme discussed above. This is somewhat surprising considering that the side-chain nitrogen atom of Asn^{706} is located within 2.8 Å of AlF in the *E*2·AlF crystal structure (Fig. 9) and that the side-chain oxygen of Asn^{706} is within bonding distance of a water molecule that coordinates the catalytic Mg^{2+} ion (indicated by *orange broken lines* in Fig. 9), although the link to Mg^{2+} might persist in mutant N706S, due to the oxygen in the serine side chain.

In the *E*2·MgF crystal structure, thought to mimic the *E*2·P_i product state, the disposition of the Asn^{706} side chain in relation to the fluoride and the water molecule coordinating the catalytic Mg^{2+} is very similar to that seen in the *E*2·AlF crystal structure (Fig. 9). Nevertheless, the inhibition data obtained with MgF (Fig. 7, *C* and *D*) showed a picture quite different from that seen for AlF. Hence, even mutation N706S lowered the affinity for MgF significantly, and the order of E183A and N706A/N706C was reversed, such that the latter two mutants displayed the most severely reduced binding affinities of the four mutants. The MgF inhibition data suggest that the Asn^{706} side chain contributes significantly to stabilization of the *E*2·P_i, product state, consistent with the *E*2·MgF crystal structure.

To understand the differential effects of Asn^{706} mutation on the binding of AlF and MgF, it could be important that there is increased negative charge density around the phosphoryl group in an associative transition state (see schematic diagram in Ref. 34). Perhaps for this reason the role of the neutral asparagine side chain is diminished during the transition and in the *E*2·AlF complex. In the *E*2·AlF crystal structure, the distance from A1 to the coordinating oxygen of Asp^{351} or the water molecule positioned by Glu^{183} is only 2.1 Å, consistent with covalent bonding (6), which means that any interaction with Asn^{706} is relatively less important for stabilization of the *E*2·AlF structure compared with *E*2·MgF, where the interaction between the protein and the fluoride does not have the character of a covalent bond.

Turning now to the mutational effects on the *E*1 states, it is clear from our nucleotide binding data (Table 1) that the Asn^{706} side chain is not critical for high affinity nucleotide binding in *E*1. Thus, the mutations of Asn^{706} had no effect on ATP binding in the absence of Mg^{2+}, and in the presence of Mg^{2+} we observed a less than 2-fold reduction of MgATP affinity, relative to wild type, for N706A and N706C, and wild type-like behavior for N706S. Likewise, the rate of phosphorylation of Ca^{2+}-saturated enzyme from [γ-^{32}P]ATP (Fig. 3*A*) as well as the binding affinity for ADP·AlF (Fig. 8) were wild type-like in N706S. The effects of the other two Asn^{706} mutations were larger, in particular N706C showed 4- to 5-fold reduced phosphorylation rate with [γ-^{32}P]ATP (Fig. 3*A*) and 15-fold reduced affinity for ADP·AlF (Fig. 8). In either of the two published crystal structures of the Ca_2E1·AlF·ADP state of Ca^{2+}-ATPase, supposed to mimic the transition state in the phosphoryl transfer from ATP (5, 7), the side chain of Asn^{706} is in a very similar position to that seen in the *E*2·MgF and *E*2·AlF crystal structures, *i.e.* within bonding distance of the fluoride and linked to the catalytic Mg^{2+} via a water molecule (*cf.* Fig. 9). The small effect of N706A and lack of effect of N706S on ADP·AlF binding suggest that Asn^{706} plays a relatively minor role in *E*1P transition state stabilization, exactly as found for the *E*2P transition state. The larger effects of mutation N706C may be due to the cysteine side chain being ionized, thereby leading to electrostatic repulsion of the γ-phosphate/AlF.

The conspicuous effects of the Asn^{706} mutations on vanadate binding to *E*2 were very similar to the effects on P_i reactivity. Both vanadate and AlF have been considered phosphoryl transition state analogs, but when one compares the results in Figs. 6 and 7*A*, it is clear that vanadate binding was much more strongly affected than AlF binding by all four mutations studied here. In particular, N706S was almost completely insensitive to vanadate and, at the same time, wild type-like with respect to inhibition by AlF. Hence, vanadate must bind and exert its inhibitory effect differently from AlF. As judged from the mutational effects, the *E*2·vanadate state seems to be a closer mimic of the enzyme with bound phosphoryl group than the enzyme complexes with fluoride com-

pounds, which may have to do with the fact that vanadate adopts a trigonal bipyramidal structure and has oxygens like phosphate, and not the strongly electronegative fluorines. The fluoride compound that resembles vanadate the most in our functional assays is BeF, with its more than 6-fold reduced apparent affinity for all four mutants relative to wild type (*cf.* Fig. 7*B*).

Besides their strong effects on P_i and vanadate reactivity, Asn^{706} mutations, including N706S, also caused significant reductions of the rates of the major protein conformational changes involved in $Ca_2E1P \rightarrow E2P$ and $E2 \rightarrow Ca_2E1$ partial reactions. It is notable that, in the *E*2·AlF and *E*2·MgF crystal structures, the side chain of Asn^{706} lines up with the TGES backbone of domain A, such that the Thr^{181} main-chain carbonyl comes close to the Asn^{706} side-chain nitrogen and the Gly^{182} main-chain amine comes close to the Asn^{706} side-chain carbonyl (interaction distances between 3.4 and 3.8 Å in the two structures, indicated by *blue broken lines* in Fig. 9). If Asn^{706} mediates similar van der Waals interactions between domains A and P in the *E*2P ground state of the native enzyme (or the residues are actually even closer and participate in hydrogen bonding), these interactions might be essential for stabilizing the docking of domain A into the catalytic site, thus explaining the slowing of the $Ca_2E1P \rightarrow E2P$ transition and destabilization of *E*2P (as well as *E*2·vanadate and *E*2·P_i) in the Asn^{706} mutants. In the functioning enzyme, most of the motions that subsequently disengage domain A from its docking site with domain P take place during the Ca^{2+} binding transition of the dephosphoenzyme ($E2 \rightarrow Ca_2E1$), although the departure of the TGES motif from the catalytic site has apparently already been initiated in *E*2 (7, 9). We observed a considerable slowing (5- to 9-fold in the absence of ATP) of the Ca^{2+} binding transition in the Asn^{706} mutants (Figs. 3*B* and 4*A*). Because in *E*2 the side chain of Asn^{706} is still within bonding distance (2.6 Å) of the main-chain carbonyl of Leu^{180}, it is not straightforward to understand why mutations of Asn^{706}, that undoubtedly disrupt this interaction, also seem to inhibit the $E2 \rightarrow Ca_2E1$ transition, rather than enhance it. Interestingly, a similar inhibition of $E2 \rightarrow Ca_2E1$ was found in E183A (10), as well as in mutants with alterations to certain other residues at the domain A-P interface (45). It appears that disruption of the normal interactions between domains A and P captures the ATPase in an *E*2-like conformation, from which departure is slow relative to the normal *E*2 state. Thus, these particular interactions seem to facilitate the normal fast cycling through *E*2.

In the light of the effects of the Asn^{706} mutations on the $Ca_2E1P \rightarrow E2P$ transition it becomes feasible to understand the changes of apparent affinity for Ca^{2+} and MgATP, which showed strikingly similar patterns (Fig. 2, *A* and *B*). As previously demonstrated by computation (36), a shift in the $K_{0.5}$ for Ca^{2+} activation of phosphorylation does not necessarily reflect a "true" change of the Ca^{2+}-binding properties. In fact, a mutant for which phosphoenzyme turnover is blocked, either by inhibition of $Ca_2E1P \rightarrow E2P$ or by inhibition of *E*2P hydrolysis, should show an *increased* apparent Ca^{2+} affinity, because lower Ca^{2+} concentrations are required for phosphoenzyme to accumulate. A similar argument holds with respect to the apparent affinity for MgATP activation of phosphorylation, and this mechanism explains the left shift of the activation curves seen for N706S in Fig. 2. For N706A and N706C, the reduced rate of phosphorylation from ATP in addition contributes to determine the apparent affinity for Ca^{2+} and MgATP, tending to right shift the curves. For N706A, the result of the two opposing effects is a $K_{0.5}$ rather similar to that of the wild type, whereas for N706C the phosphorylation rate is sufficiently low for the final result to be a right shift of the curves with increased $K_{0.5}$ relative to wild type.

In conclusion, by studying the phosphoenzyme and the binding of the three phosphate analogs, AlF, MgF, and BeF, believed to represent different states of the phosphoryl group during *E*2P dephosphorylation, we have been able to distinguish different roles of Asn^{706} and Glu^{183} during catalysis of the $E2P \leftrightarrow E2$ reaction. The extremely strong effects of the Asn^{706} mutations on the reaction of the enzyme with vanadate and P_i cannot be fully accounted for by reference to the effects on binding of the fluorides, possibly due to their strong electronegativity. However, it appears that Asn^{706} is critical for stabilizing *E*2P and, possibly therefore, also for the $Ca_2E1P \rightarrow E2P$ transition, and that it likely loses its importance in the transition state, where charge effects are greatest, but regains consequence in *E*2·P_i and *E*2. The latter conformation is only slowly transformed into Ca_2E1 in the Asn^{706} mutants. Interaction of Asn^{706} with domain A may be an important aspect of these effects.

Acknowledgments—We thank Lene Jacobsen and Karin Kracht (University of Aarhus, Aarhus, Denmark) and Irene Mardarowicz and Joy Norman (University of Cape Town, Cape Town, South Africa) for expert technical assistance.

REFERENCES

1. Hasselbach, W., and Makinose, M. (1961) *Biochem. Z.* **333,** 518–528
2. Shigekawa, M., and Dougherty, J. P. (1978) *J. Biol. Chem.* **253,** 1458–1464
3. de Meis, L., and Vianna, A. l. (1979) *Annu. Rev. Biochem.* **48,** 275–292
4. Toyoshima, C., Nakasako, M., Nomura, H., and Ogawa, H. (2000) *Nature* **405,** 647–655
5. Sørensen, T. L., Møller, J. V., and Nissen, P. (2004) *Science* **304,** 1672–1675
6. Olesen, C., Sørensen, T. L., Nielsen, R. C., Møller, J. V., and Nissen, P. (2004) *Science* **306,** 2251–2255
7. Toyoshima, C., Nomura, H., and Tsuda, T. (2004) *Nature* **432,** 361–368
8. Toyoshima, C., and Mizutani, T. (2004) *Nature* **430,** 529–535
9. Toyoshima, C., and Nomura, H. (2002) *Nature* **418,** 605–611
10. Clausen, J. D., Vilsen, B., McIntosh, D. B., Einholm, A. P., and Andersen, J. P. (2004) *Proc. Natl. Acad. Sci. U. S. A.* **101,** 2776–2781
11. Axelsen, K. B., and Palmgren, M. G. (1998) *J. Mol. Evol.* **46,** 84–101
12. Aravind, L., Galperin, M. Y., and Koonin, E. V. (1998) *Trends Biochem. Sci.* **23,** 127–129
13. Stokes, D. L., and Green, N. M. (2000) *Biophys. J.* **78,** 1765–1776
14. Wang, W., Cho, H. S., Kim, R., Jancarik, J., Yokota, H., Nguyen, H. H., Grigoriev, I. V., Wemmer, D. E., and Kim, S. H. (2002) *J. Mol. Biol.* **319,** 421–431
15. Danko, S., Yamasaki, K., Daiho, T., and Suzuki, H. (2004) *J. Biol. Chem.* **279,** 14991–14998
16. Vilsen, B., Andersen, J. P., Clarke, D. M., and MacLennan, D. H. (1989) *J. Biol. Chem.* **264,** 21024–21030
17. Clarke, D. M., Loo, T. W., and MacLennan, D. H. (1990) *J. Biol. Chem.* **265,** 14088–14092
18. Kaufman, R. J., Davies, M. V., Pathak, V. K., and Hershey, J. W. (1989) *Mol. Cell. Biol.* **9,** 946–958
19. Gluzman, Y. (1981) *Cell* **23,** 175–182
20. Chen, C., and Okayama, H. (1987) *Mol. Cell. Biol.* **7,** 2745–2752
21. Maruyama, K., and MacLennan, D. H. (1988) *Proc. Natl. Acad. Sci. U. S. A.* **85,** 3314–3318
22. Leberer, E., and Pette, D. (1986) *Biochem. J.* **235,** 67–73
23. Vilsen, B., Andersen, J. P., and MacLennan, D. H. (1991) *J. Biol. Chem.* **266,** 16157–16164
24. Sørensen, T., Vilsen, B., and Andersen, J. P. (1997) *J. Biol. Chem.* **272,** 30244–30253
25. Baginski, E. S., Foa, P. P., and Zak, B. (1967) *Clin. Chem.* **13,** 326–332
26. Andersen, J. P., Vilsen, B., Leberer, E., and MacLennan, D. H. (1989) *J. Biol. Chem.* **264,** 21018–21023
27. Sørensen, T. L., Dupont, Y., Vilsen, B., and Andersen, J. P. (2000) *J. Biol. Chem.* **275,** 5400–5408
28. Weber, K., and Osborn, M. (1969) *J. Biol. Chem.* **244,** 4406–4412
29. Clausen, J. D., and Andersen, J. P. (2003) *Biochemistry* **42,** 2585–2594
30. Murphy, A. J., and Coll, R. J. (1992) *J. Biol. Chem.* **267,** 5229–5235
31. Troullier, A., Girardet, J. L., and Dupont, Y. (1992) *J. Biol. Chem.* **267,** 22821–22829
32. Murphy, A. J., and Coll, R. J. (1993) *J. Biol. Chem.* **268,** 23307–23310
33. McIntosh, D. B., Woolley, D. G., Vilsen, B., and Andersen, J. P. (1996) *J. Biol. Chem.* **271,** 25778–25789
34. McIntosh, D. B., Woolley, D. G., MacLennan, D. H., Vilsen, B., and Andersen, J. P. (1999) *J. Biol. Chem.* **274,** 25227–25236
35. McIntosh, D. B., Clausen, J. D., Woolley, D. G., MacLennan, D. H., Vilsen, B., and Andersen, J. P. (2004) *J. Biol. Chem.* **279,** 32515–32523
36. Andersen, J. P., Sørensen, T. L., Povlsen, K., and Vilsen, B. (2001) *J. Biol. Chem.* **276,** 23312–23321
37. Inesi, G., Ma, H., Lewis, D., and Xu, C. (2004) *J. Biol. Chem.* **279,** 31629–31637

38. Ma, H., Lewis, D., Xu, C., Inesi, G., and Toyoshima, C. (2005) *Biochemistry* **44,** 8090–8100
39. Clausen, J. D., McIntosh, D. B., Woolley, D. G., and Andersen, J. P. (2001) *J. Biol. Chem.* **276,** 35741–35750
40. Guillain, F., Champeil, P., Lacapere, J. J., and Gingold, M. P. (1981) *J. Biol. Chem.* **256,** 6140–6147
41. Petithory, J. R., and Jencks, W. P. (1988) *Biochemistry* **27,** 5553–5564
42. Cantley, L. C., Jr., Cantley, L. G., and Josephson, L. (1978) *J. Biol. Chem.* **253,** 7361–7368
43. Pick, U. (1982) *J. Biol. Chem.* **257,** 6111–6119
44. Smith, R. M., and Martell, A. E. (1976) *Critical Stability Constants: Inorganic Complexes*, Plenum Press, New York
45. Wang, G., Yamasaki, K., Daiho, T., and Suzuki, H. (2005) *J. Biol. Chem.* **280,** 26508–26516

Asparagine 706 and Glutamate 183 at the Catalytic Site of Sarcoplasmic Reticulum Ca^{2+}-ATPase Play Critical but Distinct Roles in *E*2 States

Johannes D. Clausen, David B. McIntosh, David G. Woolley, Anne Nyholm Anthonisen, Bente Vilsen and Jens Peter Andersen

J. Biol. Chem. 2006, 281:9471-9481.
doi: 10.1074/jbc.M512371200 originally published online January 30, 2006